

Extraction of Temperature Distributions in Brillouin Optical Time Domain Analysis Sensors Using 2D Wiener Filter Based Matched Filter Detection

Abul Kalam Azad

Department of Electrical and Electronic Engineering, University of Dhaka, Dhaka-1000, Bangladesh

E-mail: azad@du.ac.bd

Received on 31 March 2021, Accepted for publication on 06 September 2021

ABSTRACT

In this paper, the use of 2D Wiener filter based matched filter detection (WMFD) is proposed and demonstrated for the extraction of temperature distributions in Brillouin optical time domain analysis (BOTDA) sensors. The experimental Brillouin gain spectra (BGSs) are obtained along a 38.2 km sensing fiber by adopting ten different numbers of BOTDA-trace averaging (N_{TA}). These BGSs are first denoised by applying Wiener filter (WF) to enhance the signal-to-noise ratio (SNR) of the BOTDA-traces. The improvement of trace-SNR for using WF is quantified and analyzed experimentally. The matched filter detection (MFD) which is free from time-consuming iterative optimization procedure is then applied to the denoised BGSs for the ultrafast extraction of temperature distributions along the fiber. The measurement uncertainty, spatial resolution and temperature extraction speed provided by WMFD are also analyzed in detail and compared with that provided by widely-used curve fitting method (CFM). The results show that WF can improve the trace-SNR within the range from ~ 6.78 dB to ~ 8.28 dB depending on N_{TA} . Consequently, WMFD can improve the measurement uncertainty within the range from $\sim 48.70\%$ to $\sim 59.41\%$ without sacrificing the spatial resolution as compared to CFM. Moreover, the speed in extracting temperature distributions from the experimental BGSs acquired with different N_{TA} for using WMFD can be improved within the range from ~ 47.36 times to ~ 50.69 times as compared to that for using CFM. Thus, the proposed WMFD can be an effective approach for highly accurate and ultrafast extraction of temperature distributions along the sensing fiber.

Keywords: Distributed fiber-optic sensors, Wiener filter, Matched filter detection, Least-squares curve fitting, Data interpolation, Lorentzian function.

1. Introduction

Distributed fiber-optic sensors furnish inimitable facility to measure various physical parameters, such as temperature, vibration and strain in hazardous operating environment [1 - 4]. Among various fiber-optic sensor technologies, Brillouin optical time domain analysis (BOTDA) sensors facilitate the long range measurement of temperature with good spatial resolution and low uncertainty [5 - 7]. In the Brillouin gain arrangement of BOTDA sensors, the pump and the probe waves are launched through two opposite ends of a sensing fiber. Owing to the interaction of these two oppositely directed waves throughout the fiber, the probe wave becomes amplified. The amplified probe wave at different pump-probe frequency differences is obtained step-by-step and recorded as BOTDA-traces along the fiber. These BOTDA-traces are finally used to recreate the local Brillouin gain spectra (BGSs) along the fiber. The peak Brillouin gain in such a local BGS occurs at a particular pump-probe frequency difference which is identical to the local Brillouin frequency shift (BFS) of the fiber. This BFS of the local BGS changes linearly with local temperature [7, 8]. Consequently, the BGSs along the fiber are processed to determine the local BFSs and the linear BFS-temperature characteristics of the fiber are used to convert such local BFSs to temperature distribution along the fiber.

The simplest and fastest way for estimating the BFSs of the experimental BGSs is to use maximum finding method, in which BFSs are determined just by finding the frequencies of the peak amplitudes of the BGSs [8]. However, such method provides large uncertainty in the estimation of BFSs as the BGSs obtained from BOTDA experiment are noisy

and the peak Brillouin frequencies of such noisy BGSs shift greatly from their original BFSs due to the random distribution of noise. To overcome this limitation, the curve fitting method (CFM) is usually employed in which a suitable model function is fitted on to the experimental BGSs [7-10]. Then, the BFSs of such BGSs are presumed to be the frequencies of the peak amplitudes of the fitted curves. However, the uncertainty in temperature extraction provided by CFM is quite large, especially for low SNR at the end of a long fiber [9, 10]. Moreover, the CFM utilizes iterative optimization procedure that takes long time to estimate BFSs, especially for large number of BGSs along a long fiber [8, 11]. Consequently, the use of CFM to process BGSs acquired from BOTDA sensor is limited in practical applications where fast and accurate extraction of temperature distribution is not utterly essential.

In theory, the measurement uncertainty of BOTDA sensors predominantly depends on the SNR of the experimental BGSs [10, 12]. To enhance such SNR to a desired level, averaging of BOTDA-traces is a frequently-used and fruitful mechanism [10, 13]. In such mechanism, thousands of BOTDA-traces are obtained and averaged during BOTDA experiment for the acquisition of a single trace. Consequently, the time required for the acquisition of BGSs along the fiber from BOTDA experiment increases greatly if large number of trace averaging (N_{TA}) is used. An alternative mechanism is to use smaller N_{TA} during the acquisition of experimental BGSs, and then to denoise such noisy BGSs by dint of a suitable denoising algorithm. For this, the use of different denoising algorithms is reported recently which includes non-local means [14, 15],

anisotropic diffusion [16], cross-correlation [13, 17] and wavelet transform [12, 18]. Surprisingly, the effects of these denoising algorithms on the spatial resolution of the BOTDA sensors and that on the speed of processing experimental BGSs are not addressed and analyzed rigorously with proper experimental results in literature.

In this paper, the use of 2D Wiener filter based matched filter detection (WMFD) is proposed and demonstrated for BOTDA sensors to extract temperature distributions along a 38.2 km sensing fiber. The benefits of using WMFD are analyzed in detail with reference to measurement uncertainty, spatial resolution and BGSs processing speed. The performance of WMFD in extracting temperature distributions for BOTDA sensors is also compared with that of commonly-used curve fitting method (CFM).

2. Acquisition and Processing of Experimental BGSs

2.1 Experimental Setup for the Acquisition of BGSs

The experimental setup of a standard BOTDA sensor [7, 19] is shown in Fig. 1. The leftmost device in the setup is a continuous-wave (CW) tunable laser source which supplies light wave at 1550 nm. The output of the laser source is divided by a coupler to provide CW light waves through the upper and lower arms in the experimental setup. The polarization state of the light wave through the upper arm is controlled by the polarization controller (PC1). The electro-optic modulator (EOM1) inserted in the upper arm utilizes a radio-frequency generator (RFG) to modulate the CW wave and provides double-sideband suppressed-carrier (DSB-SC) probe wave. The variable optical attenuator (VOA) in the upper arm is applied to adjust the power of the DSB-SC probe wave. The DSB-SC probe wave is then passed through an optical isolator which allows the launching of this wave through the rearmost end of the 38.2 km long sensing fiber but blocks the propagation of light in the reverse direction coming from the fiber toward this upper arm. The rearmost ~ 0.6 km segment of the 38.2 km fiber is manually unrolled from the fiber mandrel and heated inside the constant temperature oven.

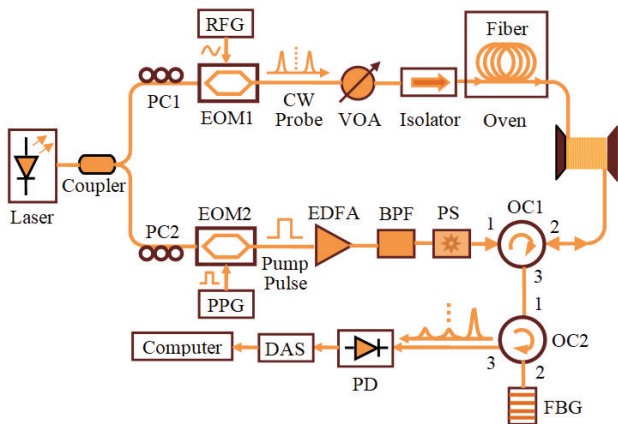


Fig. 1. Experimental setup of a standard BOTDA sensor.

In the BOTDA setup, the polarization state of the CW wave provided by the coupler through the lower arm is also

controlled by the second polarization controller (PC2). Then, another electro-optic modulator (EOM2) makes use of a pulse-pattern generator (PPG) to modulate the CW wave and generates pump-pulses in this lower arm. The width of these pump-pulses is fixed to be 20 ns to attain 2 m spatial resolution of the sensor. The power of the pump-pulses is amplified by applying an erbium-doped fiber amplifier (EDFA). Besides the amplified pump-pulses, the EDFA also outputs amplified spontaneous emission (ASE) noise that is filtered out by inserting the band-pass filter (BPF) in this lower arm. Then, the polarization scrambler (PS) in the lower arm is used to randomize the state of the polarization over time so that the polarization-induced fading of Brillouin gain is minimized. The optical circulators (OC1 and OC2) in Fig. 1 work in such a way that the light arriving port '1' departs from port '2' and that arriving port '2' departs from port '3'. As a result, the OC1 used in the lower arm permits the launching of pump-pulses through the foremost end of the sensing fiber.

In the BOTDA experimental setup shown in Fig. 1, the probe and pump waves propagating in the reverse directions interact in the sensing fiber. Owing to this interaction, the pump wave delivers a portion of its power to the probe wave and the DSB-SC probe wave gets amplified. The OC1 and OC2 used in the setup allow the propagation of this amplified DSB-SC probe wave to the fiber Bragg grating (FBG) filter for selecting the desired low-frequency sideband only. The photo-detector (PD) is then used to detect this low-frequency sideband. At a given pump-probe frequency difference, the data acquisition system (DAS) acquires one BOTDA-trace along the fiber by sampling the output of the PD at a sampling interval of 0.4 m. By subsequently scanning the pump-probe frequency differences within the frequency-range from $\nu_{start} = 10.76$ GHz to $\nu_{stop} = 11.01$ GHz at a step of $\nu_{step} = 1$ MHz, the BOTDA-traces are acquired and stored in the computer. These traces are finally used to recreate the local BGSs along the fiber.

2.2 Wiener Filter (WF) Based BGSs Denoising

The Wiener filter (WF) is used for denoising signals and images in science, engineering and biomedical applications [20 - 23]. In image denoising applications, locally adaptive 2D WF is extensively used due to its ability to preserve the edges and the crucial high-frequency components of the images [22, 23]. In this study, the noisy BGSs along the sensing fiber acquired from BOTDA experiment is considered as a 2D image $E(p, q)$ and then pixel-wise adaptive 2D Wiener filter is used to denoise it. In such denoising process, neighborhood pixels are used to find local image mean and local image variance. The local image mean (μ) for each pixel using its P -by- Q neighborhood pixels in WF [23] is computed by

$$\mu = \frac{1}{PQ} \sum_{p,q \in \rho} E(p, q) \quad (1)$$

whereas the local image variance (σ^2) is computed by

$$\sigma^2 = \frac{1}{PQ} \sum_{p,q \in \rho} E^2(p,q) - \mu^2. \quad (2)$$

In Eq. (1) and Eq. (2), ρ is the P -by- Q local neighborhood of each pixel in $E(v, g)$. The filtered (i.e., denoised) value $D(p, q)$ of each pixel $E(p, q)$ in $E(v, g)$ is then estimated to be

$$D(p, q) = \mu + \frac{\sigma^2 - \sigma_n^2}{\sigma^2} [E(p, q) - \mu] \quad (3)$$

where σ_n^2 is the noise variance which is calculated to be the mean of all local estimated variances in this study. It is seen in Eq. (3) that the image denoising operation of WF is tailored in accordance with the variance (σ^2) of the local image. For a larger value of σ^2 , the WF performs lesser smoothing whereas more smoothing is performed for a smaller value of σ^2 . Consequently, WF can preserve the edges and high-frequency areas of $E(v, g)$ which, in turn, helps to preserve the spatial resolution of the BOTDA sensors.

Once the process of denoising of the image $E(v, g)$ comprising the experimental BGSs is over, the denoised image $D(v, g)$ is obtained which contains the denoised BGSs along the fiber. Next, the MFD is employed to estimate the BFSs of the denoised BGSs along the sensing fiber.

2.3 Matched Filter Detection (MFD)

The matched filter detection (MFD) is successfully used in communication receivers for maximizing the output SNR [24 - 27]. In MFD, the impulse response of the used matched filter must be the folded version of the information signal delayed by the symbol duration [26, 27]. In BOTDA experiment, the BFSs of the local BGSs along the fiber vary with local temperatures, whose distribution are not known priori and needs to be determined after processing the BGSs. Thus, for simplicity, the impulse response $g_f(v)$ of the matched filter used in this study is selected to be fixed which does not vary in accordance with the BFSs of the experimental BGSs along the fiber. In addition, the experimental BGSs $g_E(v)$ along the fiber acquired from BOTDA experiment are ideally modeled by Lorentzian function [7 - 9]. Consequently, the $g_E(v)$ along the fiber as well as the $g_f(v)$ used for MFD is also modeled with Lorentzian function given respectively by

$$g_E(v) = \frac{g_{BE}}{1 + 4[(v - v_{BE}) / (\Delta v_{BE})]^2}. \quad (4)$$

$$g_F(v) = \frac{g_{BF}}{1 + 4[(v - v_{BF}) / (\Delta v_{BF})]^2}. \quad (5)$$

In Eq. (4) and Eq. (5), g_{BE} and g_{BF} are the peak amplitudes, v_{BE} and v_{BF} are the BFSs; and Δv_{BE} and Δv_{BF} are the full-widths at half-maximum (FWHMs) of the experimental BGSs and impulse response of the matched filter respectively.

In the MFD, each of the local BGSs $g_E(v)$ along the fiber is passed through the matched filter having the impulse response of $g_F(v)$. To simulate $g_F(v)$, the frequency (v) in Eq. (5) ranges from $v_{start} = 10.76$ GHz to $v_{stop} = 11.01$ GHz, the similar range used to acquire BGSs from the BOTDA sensor. The BFS in Eq. (5) is set at the middle of v_{start} and v_{stop} (i.e., $v_{BF} = 10.885$ GHz) and peak amplitude is set at $g_{BF} = 1$. In Eq. (5), the FWHM of $g_F(v)$ is set at $\Delta v_{BF} = 50$ MHz (i.e., roughly equal to the FWHMs of the experimental BGSs) considering the used pump-pulses having width of 20 ns [7, 28]. Then, the output $g_C(v)$ of the matched filter is obtained by convolving $g_E(v)$ and $g_F(v)$. The $g_C(v)$ is also assumed to be a Lorentzian function, especially in the vicinity of its peak. Thus, $g_C(v)$ is given by

$$g_C(v) = \frac{g_{BC}}{1 + 4[(v - v_{BC}) / (\Delta v_{BC})]^2}. \quad (6)$$

In Eq. (6), g_{BC} is the peak amplitude, v_{BC} is the BFS, and Δv_{BC} is the FWHM of the convolved BGS. The convolution operation between a clean BGS $g_E(v)$ having the BFS of v_{BE} and the impulse response $g_F(v)$ of the matched filter having the BFS of v_{BF} produces the convolved BGS $g_C(v)$ having BFS of v_{BC} as illustrated in Fig. 2. For the comparison, the result of such convolution operation between the noisy version of $g_E(v)$ and the same $g_F(v)$ is also shown in Fig. 2.

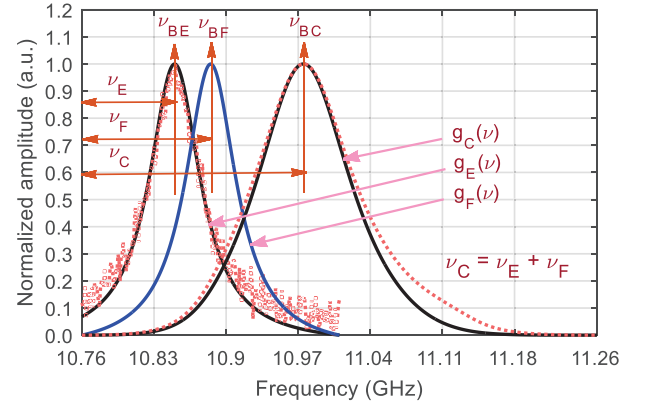


Fig. 2. Graphical illustration of matched filter detection (MFD).

It is noticed in Fig. 2 that the convolved BGSs $g_C(v)$ obtained for both the clean $g_E(v)$ and its noisy version are almost noise free, especially in the vicinity of the peaks of $g_C(v)$. As a result, the BFS v_{BC} of the convolved BGS can now simply be estimated accurately by finding the frequency ($v = v_{BC}$) having peak amplitude in $g_C(v)$. Such process of finding v_{BC} having maximum amplitude does not employ any iterative optimization procedure, and thus very fast. It is also observed in Fig. 2 that the frequency differences from the BFSs of the three BGSs from v_{start} (i.e., 10.76 GHz) are interrelated by

$$v_C = v_E + v_F \quad (7)$$

where $v_C = v_{BC} - v_{start}$, $v_E = v_{BE} - v_{start}$ and $v_F = v_{BF} - v_{start}$. Putting these values in Eq. (7) gives

$$v_{BE} = v_{start} + (v_{BC} - v_{BF}). \quad (8)$$

In Eq. (8), $v_{start} = 10.76$ GHz, v_{BF} is set at $= 10.885$ GHz and v_{BC} is estimated just by finding the frequency at peak amplitude. The use of Eq. (8) thus allows the fast and accurate estimation of BFSs of experimental BGSs along the fiber.

The uncertainty in extracting temperature distributions using MFD becomes larger if frequency scanning step (v_{step}) used to acquire BGSs from the BOTDA experiment is also larger and v_{BC} of $g_C(v)$ in Eq. (8) is determined by finding the frequency at peak amplitude. For example, $v_{step} = 1$ MHz within the scanning frequency ranging from $v_{start} = 10.76$ GHz to $v_{stop} = 11.01$ GHz used in this study introduces an uncertainty in estimating the v_{BC} within the range from 0 MHz to 0.5 MHz. Consequently, the estimation of v_{BE} of $g_E(v)$ using Eq. (8) also suffers from the uncertainty within the same range. This uncertainty in extracting BFSs of the noisy experimental BGSs along the fiber ultimately affects the uncertainty in extracting temperature distributions due to the linear relationship between BFS and temperature. The reduction of such uncertainty to a negligible level requires the use of very small v_{step} that, in turn, lengthens the acquisition time of BGSs from BOTDA experiment. To minimize this problem, an alternative technique of data interpolation is used in this study to up-sample the experimental BGSs along the fiber acquired at $v_{step} = 1$ MHz. To perform this with an interpolation factor of I_F , $I_F - 1$ zeros are inserted between two successive sample points on each BGS and the triangle window based low-pass filter is then applied to filter out the up-sampled BGSs.

2.4 Curve Fitting Method (CFM)

In CFM, the nonlinear least-squares fitting is used to extract BFSs from the experimental BGSs along the fiber [7, 12]. For this, the Lorentzian function given by Eq. (4) is used to fit sample points $(g_{E1}, v_1), (g_{E2}, v_2), \dots, (g_{En}, v_n)$ of each experimental BGS along the fiber. Such fitting is achieved by minimizing the error function given by

$$E(\hat{u}) = \sum_{i=1}^n [g_{Ei} - g_E(v_i, \hat{u})]^2 \quad (9)$$

where the vector \hat{u} comprising g_{BE} , v_{BE} and Δv_{BE} of Eq. (4) is updated and optimized iteratively and the v_{BE} of the fitted curve is presumed to be the BFS of the experimental BGS. The process of CFM is explicitly described in Ref [7, 8].

3. Experimental Results and Discussion

In this demonstration, a 38.2 km fiber span is placed in the BOTDA setup shown in Fig. 1. The rearmost part of ~ 0.6 km fiber from this fiber span is positioned in the interior of a constant temperature oven. The remaining part of the fiber is kept to the exterior of the oven at room temperature of ~ 25 °C. The rearmost ~ 0.6 km fiber is heated each time at one of the two different oven temperatures of 40 °C and 60 °C. To acquire BGSs with different levels of noise, the number of trace averaging (N_{TA}) used during the acquisition of BGSs at each oven temperature is varied from $N_{TA} = 100$ to $N_{TA} = 1000$ at a step of 100. The BGSs acquired from BOTDA

experiment at each of the two different oven temperatures and ten different N_{TA} are first denoised by applying 2D Wiener filter (WF) as depicted in section 2.2 To apply MFD, the impulse response $g_f(v)$ of the matched filter is simulated by utilizing Eq. (5) as described in section 2.3 The $g_f(v)$ is then convolved individually with each of the denoised BGSs obtained after applying WF to the experimental BGSs acquired at different oven temperatures and N_{TA} . For instances, the distribution of experimental BGSs acquired at $N_{TA} = 500$ for the oven temperature of 60 °C is shown in Fig. 3(a) and that of denoised BGSs obtained after applying WF to the experimental BGSs in Fig. 3(a) is shown in Fig. 3(b). The distribution of convolved BGSs obtained after convolving $g_f(v)$ and denoised BGSs in Fig. 3(b) is also shown in Fig. 3(c).

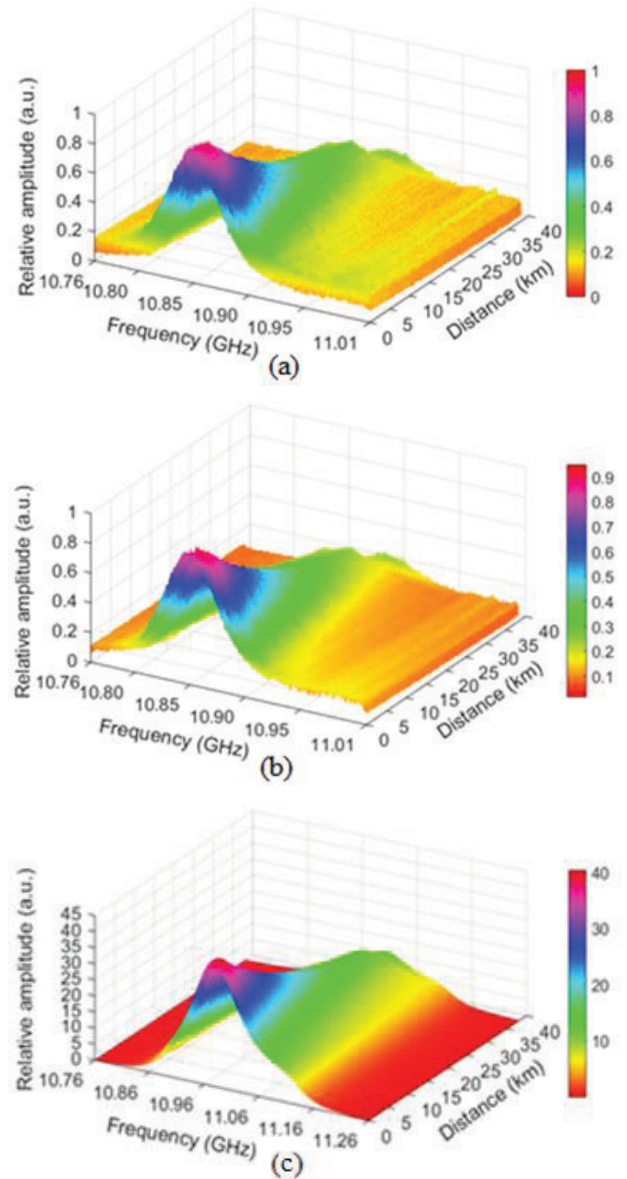


Fig. 3. Distributions of (a) experimental noisy BGSs, (b) BGSs denoised by the Wiener filter, and (c) convolved denoised BGSs along the 38.2 km fiber in which the rearmost ~ 0.6 km fiber segment is heated at 60 °C.

The comparison among the distribution of BGSs along the fiber in Fig. 3(a) with that in Fig. 3(b) reveals that the used WF can noticeably reduce noise from the experimental BGSs. To observe the denoising performance of WF more clearly, the BOTDA-trace at 10.858 GHz representing ~ 25 °C from the experimental noisy BGSs in Fig. 3(a) without applying WF and the corresponding BOTDA-trace of the BGSs denoised with WF in Fig. 3(b) are plotted in Fig. 4. It is now clearly remarked in Fig. 4 that the fluctuation of relative trace amplitude with applying WF is significantly smaller than that without applying WF. As a result, the level of noise in the experimental BOTDA-trace is also reduced significantly due to the use of WF. In fact, the lower noise level in each of the BOTDA-traces acquired at different scanning frequencies after applying WF constitutes the distribution of denoised BGSs along the fiber in Fig. 3(b).

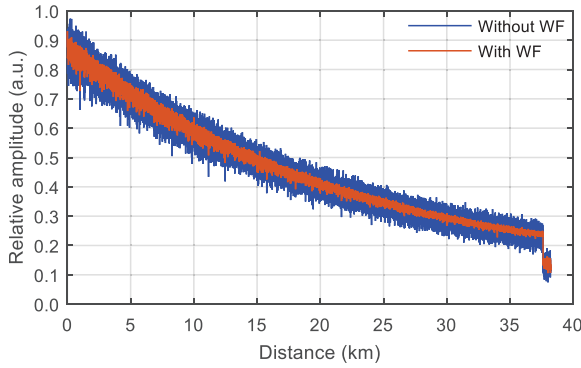


Fig. 4. Experimental and denoised BOTDA-traces along the fiber before and after applying the Wiener filter.

To evaluate the denoising performance of WF quantitatively for the BGSs acquired with different N_{TA} , the SNRs of the experimental BOTDA-traces and their corresponding denoised BOTDA-traces are computed. Such SNRs are computed for the traces along the rearmost 0.5 km fiber (i.e., worst SNR) heated each time at 40 °C and 60 °C. For this, the BOTDA-traces at 10.873 GHz corresponding to the peak Brillouin gains of BGSs at 40 °C are chosen for each of the ten different N_{TA} . Similarly, the BOTDA traces at 10.892 GHz are selected for oven temperature of 60 °C. The SNR of each of such traces at different N_{TA} and temperatures is separately calculated to be the ratio of the average to standard deviation of such trace amplitudes [19]. For a particular N_{TA} , two nearly-equal SNRs are obtained for two different temperatures. These two SNRs are averaged to approximate the SNR at that N_{TA} . The variation of trace-SNR with N_{TA} is displayed in Fig. 5.

It is observed in Fig. 5 that the SNR of experimental trace without applying WF is the lowest at $N_{TA} = 100$, the smallest N_{TA} adopted in this study. As a consequence, the improvement of SNR due to applying WF at $N_{TA} = 100$ is also the highest which is ~ 8.28 dB in this case. In addition, the SNR of the experimental traces without applying WF increases when such traces are acquired with larger N_{TA} . Consequently, the improvement of SNR for applying WF at larger N_{TA} decreases slightly and becomes ~ 6.78 dB at $N_{TA} = 1000$, the largest N_{TA} adopted in this study. However, it is clear from Fig. 5 that the

trace-SNR with the use of WF at each of the ten different N_{TA} is significantly better than that without the use of WF.

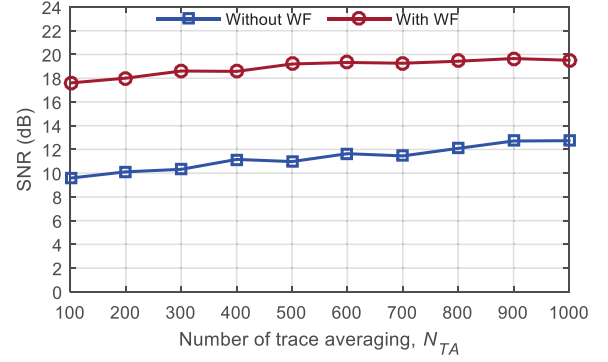


Fig. 5. The trace-SNRs for the rearmost 0.5 km heated segment of the 38.2 km fiber before and after applying the Wiener filter.

Next, the MFD in WMFD is applied to the denoised BGSs for extracting temperature distributions along the fiber. For the purpose of comparison, the temperature distributions from the experimental BGSs are also extracted by using CFM. For extracting the distributions of temperature from the BFSs of the BGSs along the fiber, the BFS-temperature characteristics (i.e., slope of ~ 0.97497 MHz/°C and intercept of ~ 10.83415 GHz) of the same fiber used in Ref. [7] and in this study are utilized. For instances, the distributions of temperature given by WMFD and that given by CFM are shown in Fig. 6. It is worth to mention that the temperature distributions given by WMFD in Fig. 6(a) utilize a data interpolation factor of $I_F = 5$.

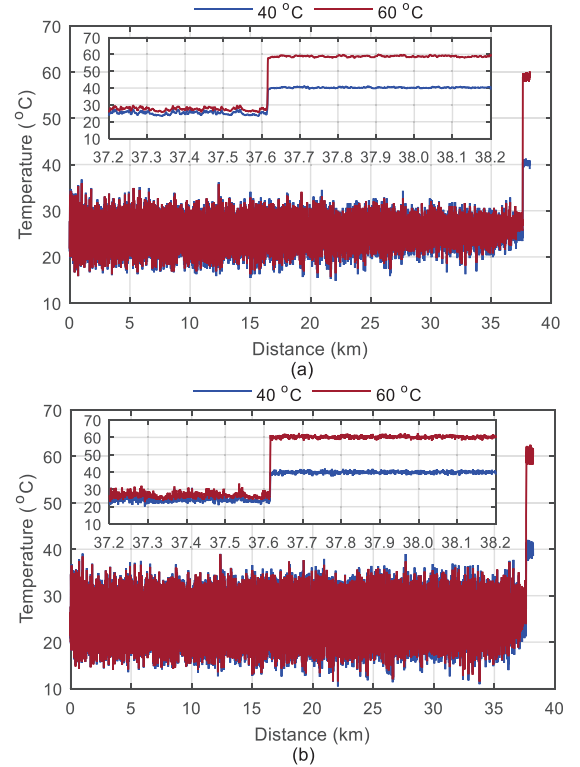


Fig. 6. (a) WMFD and (b) CFM extracted temperature distributions along the 38.2 km fiber with the rearmost ~ 0.6 km fiber segment heated at 40 °C and 60 °C. Inset: Temperature distributions along the last 1 km fiber segment.

It is seen in Fig. 6(a) that the WMFD can properly extract the distributions of temperature from the experimental BGSs along the fiber. In addition, the fluctuation of temperatures along the fiber for using WMFD in Fig. 6(a) is much smaller than that for using CFM in Fig. 6(b). As a result, WMFD can provide much lower uncertainty in extracting temperature distributions as compared to CFM.

Next, the effect of applying WMFD on the spatial resolution of the BOTDA sensor is observed and verified. For this, the temperature distributions provided by WMFD and CFM along the 10 m fiber segment (i.e., from 37.610 km to 37.620 km) where the sharp transitions of temperature distributions take place from room temperature of ~ 25 °C to oven temperatures of 40 °C and 60 °C are plotted in Fig. 7. The results show that both WMFD and CFM can preserve the 2 m spatial resolution of the sensor which is desirable for adopting 20 ns pump-pulses in BOTDA experimental setup shown in Fig. 1.

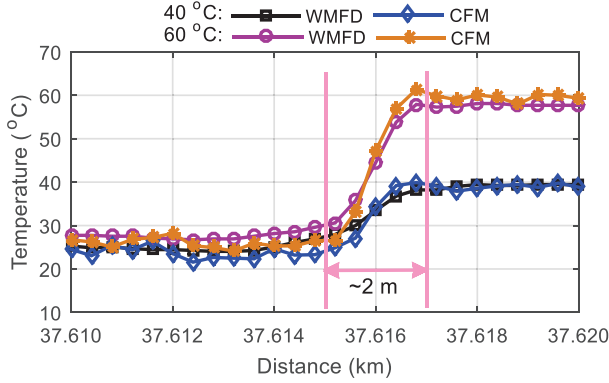


Fig. 7. Transitions of temperature distributions along the fiber segment starting from 37.610 km to 37.620 km that show the preservation of 2 m spatial resolution.

The distributions of temperature in Fig. 6 reveal that WMFD can render much smaller fluctuation in extracting temperature distributions as compared to CFM. To verify this quantitatively, the performance of WMFD is also compared with that of CFM in term of uncertainty in extracting temperature distributions along the fiber. To compute such uncertainty, the distributions of temperature extracted by WMFD and CFM along the rearmost 0.5 km fiber segment heated inside the oven are considered. The uncertainties provided by WMFD or CFM at ten different N_{TA} and two different oven temperatures are separately computed to be the standard deviation of the temperatures along this 0.5 km fiber segment. Again, two nearly-equal uncertainties are obtained for two different oven temperatures of 40 °C and 60 °C. These nearly-equal uncertainties are averaged to estimate the uncertainty provided by WMFD or CFM at a particular N_{TA} . The uncertainties calculated for using WMFD with $I_F = 5$ and that for using CFM are shown in Fig. 8.

The results presented in Fig. 8 disclose that the uncertainties in extracting temperature distributions provided by WMFD as well as CFM reduce gradually if larger N_{TA} (i.e., higher SNR) is adopted in BOTDA

experiment to acquire BGSs. The results in Fig. 8 also demonstrate that the uncertainties provided by WMFD are significantly lower than that provided by CFM at each of the ten different N_{TA} . For examples, the uncertainties for using WMFD at $N_{TA} = 500$ is ~ 0.36 °C which is much lower than ~ 0.74 °C for using CFM at the same N_{TA} . To examine the improvement of performance of the BOTDA sensor for using WMFD, the improvement of uncertainty is also computed in percentage (%) by comparing the uncertainties provided by WMFD for $I_F = 5$ with that provided by CFM. The results are shown in Fig. 9.

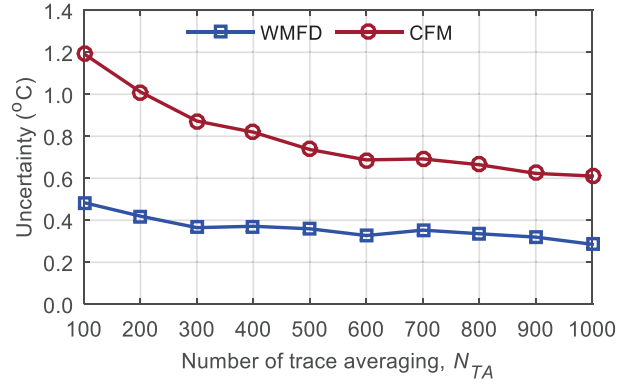


Fig. 8. Variation of uncertainty in the extraction of temperature distributions with N_{TA} used to acquire BGSs.

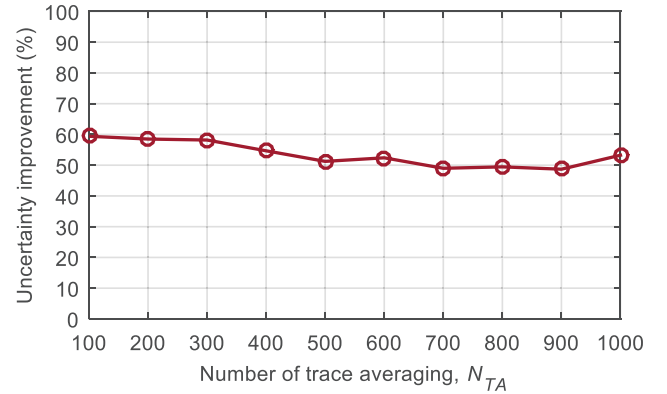


Fig. 9. Variation of uncertainty improvement for using WMFD compared to CFM in the extraction of temperature distributions with N_{TA} used to acquire BGSs.

It is observed in Fig. 9 that the improvement of uncertainty for using WMFD compared to CFM at different N_{TA} varies within the range from $\sim 48.70\%$ to $\sim 59.41\%$. For example, the uncertainties in Fig. 8 provided by WMFD and CFM at $N_{TA} = 200$ are ~ 0.42 °C and ~ 1.01 °C respectively. Consequently, the uncertainty for using WMFD at $N_{TA} = 200$ is improved by $\sim 58.42\%$ as compared to CFM as shown in Fig. 9. However, the results in Fig. 9 also show a little decrease in uncertainty improvement for the BGSs acquired at larger N_{TA} . This is reasonable because at larger N_{TA} , the trace-SNRs of the experimental BGSs are already higher than that at smaller N_{TA} as shown in Fig. 5. As a result, the improvement of uncertainty at larger N_{TA} in Fig. 9 is also lower as compared to that at larger N_{TA} used in this study. However, the results in Fig. 8 and Fig. 9 confirm the

superiority of WMFD over CFM at each of the ten different N_{TA} regarding the uncertainty in extracting temperature distributions.

The practical implementation of BOTDA sensors entails the fast and accurate extraction of temperature distributions along a multiple tens of kilometers sensing fiber. The acquisition time of BGSs from BOTDA experiment at larger N_{TA} for such long fiber is noticeably long. To make BOTDA sensors suitable for faster operation, a lower N_{TA} should be used which in turn provides BGSs with lower trace-SNR and thus increase the measurement uncertainty. In addition to the faster acquisition of BGSs, the processing time required to extract temperature distributions from the acquired BGSs should also be as short as possible. In this study, the use of WF in WMFD for denoising experimental BGSs facilitates to reduce the uncertainty of BOTDA sensors. However, as a preprocessing tool, WF also includes additional processing time in the extraction of temperature distributions to WMFD. The effect of denoising experimental BGSs by using WF on the processing time to extract temperature distributions by using WMFD is presented and analyzed next.

To analyze the processing time for extracting temperature distributions along the fiber, the runtimes for using both WF and MFD in WMFD are recorded separately where a data interpolation factor of $I_F = 5$ is used in MFD. Then, the proportion of runtime required for using WF and that for using MFD in WMFD at a particular N_{TA} are expressed in percentage (%). The results are shown in Fig. 10.

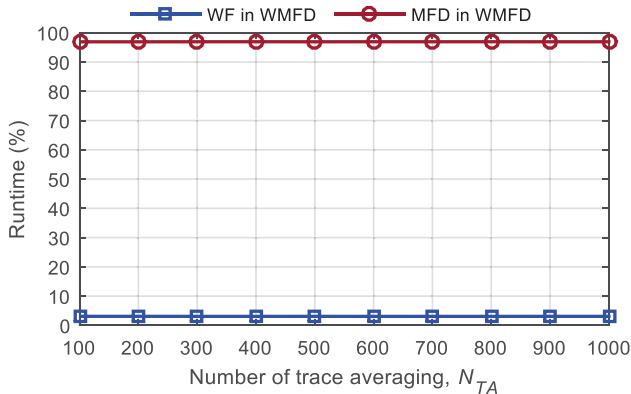


Fig. 10. Proportions of runtime required by WF and MFD in WMFD for extracting temperature distributions along the fiber.

The results presented in Fig. 10 indicate that the percentage of runtime required by WF and that required by MFD in WMFD do not vary remarkably with N_{TA} . It can also be observed in Fig. 10 that the average runtimes required by WF and MFD respectively are $\sim 3.09\%$ and $\sim 96.91\%$ of total runtime required by WMFD. Consequently, the results in Fig. 3 divulge that the runtimes required by WF is significantly smaller than that required by MFD in WMFD, i.e., WF does not add significant preprocessing time to WMFD. The speeds of extracting temperature distributions by using WMFD and that by using CFM are also compared in term of relative runtime. The relative runtime at a particular N_{TA} is computed by dividing the runtime of CFM

by that of WMFD with $I_F = 5$. The computed relative runtimes are shown in Fig. 11.

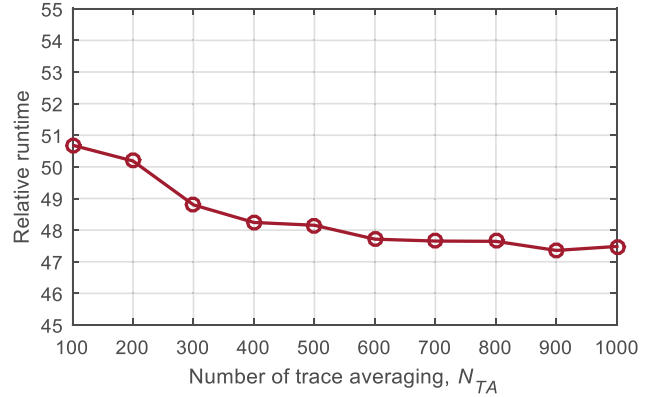


Fig. 11. Relative runtime of CFM to WMFD in extracting temperature distributions along the fiber.

The advantage of using WMFD for the fast extraction of temperature distributions in BOTDA sensors is revealed in Fig. 11. As shown in Fig. 11, the relative runtime of CFM to WMFD at $N_{TA} = 100$ is ~ 50.69 . This means that the extraction of temperature distribution by using WMFD at $N_{TA} = 100$ is ~ 50.69 times faster than that by using CFM. It is also observed in Fig. 11 that the relative runtime of CFM to WMFD decreases slowly when larger N_{TA} is used to acquire the BGSs from the BOTDA experiment and minimum relative runtime obtained is ~ 47.36 in this study. This decrease of relative runtime is due to the fact that the iterative optimization procedure involved in CFM utilizes relatively smaller number of iterations (i.e., shorter runtime) to optimize the model parameters for extracting temperature distributions from the BGSs acquired at larger N_{TA} (i.e., higher SNR) but the runtimes required by WF and MFD in WMFD are independent of N_{TA} as shown in Fig. 10.

The results presented in Fig. 9 and Fig. 11 unveil that the uncertainty as well as runtime in extracting temperature distribution can be reduced by more than $\sim 48.70\%$ and ~ 47.36 times by using WMFD with a data interpolation factor of $I_F = 5$ as compared to CFM. In this study, the improvements of uncertainty in extracting temperature distributions for adopting ten different I_F in WMFD are also computed and analyzed. For this analysis, the uncertainty in extracting temperature distribution for using WMFD with each of the ten different I_F starting from $I_F = 1$ to $I_F = 10$ at each of the ten different N_{TA} is computed and compared with that for using WMFD with $I_F = 1$ (i.e., no data interpolation). The results are plotted in Fig. 12 for four different numbers of trace averaging of $N_{TA} = 100, 200, 500$ and 1000 .

The results in Fig. 12 show that the use of larger I_F in WMFD provides more improvement of uncertainty in extracting temperature distributions from the BGSs acquired at different N_{TA} . For instances, the improvements of uncertainty at $N_{TA} = 500$ is $\sim 14.16\%$ for using WMFD with $I_F = 2$ which becomes $\sim 25.75\%$ and $\sim 27.32\%$ with $I_F = 5$ and $I_F = 8$ respectively as compared to $I_F = 1$. The results in Fig. 12 also indicate that the improvement of uncertainty

increases rapidly for smaller I_F (e.g., $I_F = 2$ to 5) and becomes almost constant for larger I_F (e.g., $I_F = 6$ to 10). It should be noted here again that the experimental BGSs processed in this study is acquired from BOTDA experiment at a frequency step of $v_{step} = 1$ MHz. The use of $I_F = 5$ is equivalent to adopt $v_{step} = 0.2$ MHz in BOTDA experiment which is much smaller. As a result, the improvement of uncertainty for using larger I_F beyond $I_F = 5$ cannot improve the uncertainty significantly. It is also noticed in Fig. 12 that the effects of different I_F on the experimental BGSs acquired at different N_{TA} is not identical. This is because the uncertainty improvement at smaller N_{TA} is mainly dominated by the level of noise in the experimental BGSs rather than I_F adopted in WMFD.

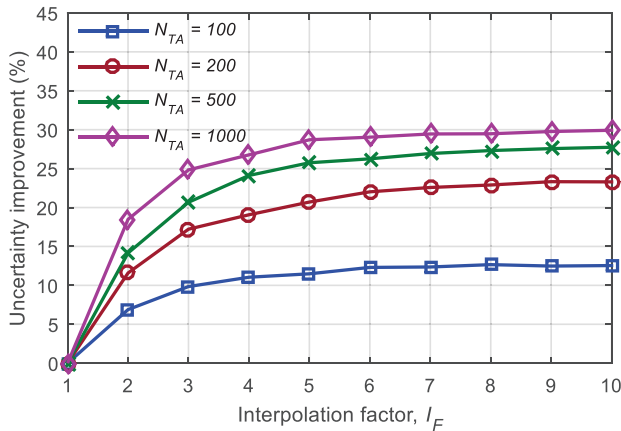


Fig. 12. Variation of uncertainty improvement in extracting temperature distributions using WMFD with different interpolation factors of I_F relative to $I_F = 1$.

The results presented in Fig. 12 signify that adopting larger data interpolation factor (e.g., $I_F > 1$) in WMFD facilitates more uncertainty improvement in the extraction of temperature distributions. However, the use of larger I_F also affects the runtime of WMFD in extracting temperature distributions. This effect is analyzed next in term of relative runtime for adopting ten different I_F in WMFD. For such analysis, the runtime in extracting temperature distributions for using WMFD with each of the ten different I_F starting from $I_F = 1$ to $I_F = 10$ at each of the ten different N_{TA} is computed and compared with that for using WMFD with $I_F = 1$. The results are presented in Fig. 13 for four different numbers of trace averaging of $N_{TA} = 100, 200, 500$ and 1000.

It is observe in Fig. 13 that the relative runtime of WMFD is independent of N_{TA} and increases rapidly if larger I_F is adopted in WMFD. For examples, the relative runtimes of WMFD with $I_F = 2, 5$ and 8 are $\sim 1.44, \sim 4.64$ and ~ 8.58 respectively as compared to that with $I_F = 1$. This means that temperature extraction using WMFD with $I_F = 2, 5$ and 8 respectively are ~ 1.44 times, ~ 4.64 times and ~ 8.58 times slower than that using WMFD with $I_F = 1$. This is because the process of data interpolation adopting larger I_F takes relatively longer time as compared to that adopting smaller I_F . Moreover, the number of data points on each BGS also increases if larger I_F is adopted which, in turn, affects other subsequent processing stages in WMFD. Consequently, the

runtime of WMFD at larger I_F becomes longer. Referring to Fig. 13, it is noteworthy that the extraction of temperature distributions using WMFD with $I_F = 5$ is ~ 4.64 times slower than that with $I_F = 1$. However, the extraction of temperature distributions from the experimental BGSs along the sensing fiber for using WMFD with $I_F = 5$ is more than ~ 47.36 times faster than that for using CFM as shown in Fig. 11. Consequently, the temperature extraction for using WMFD with $I_F = 1$ is more than ~ 219.75 times faster than that for using CFM.

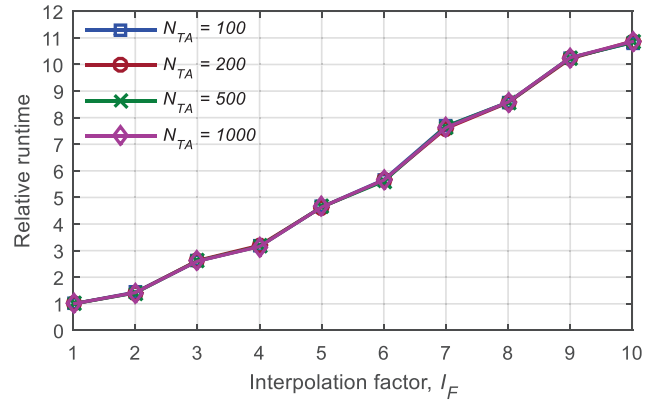


Fig. 13. Variation of relative runtime in extracting temperature distributions using WMFD with different interpolation factors of I_F relative to $I_F = 1$.

4. Conclusions

A comprehensive analysis of 2D Wiener filter based matched filter detection (WMFD) is proposed and demonstrated for extracting temperature distributions along a 38.2 km sensing fiber in BOTDA sensors. The performance of WMFD is explored systematically for the experimental BGSs obtained from BOTDA experiment with different numbers of trace averaging. The results attained illustrate that WMFD can provide much reduced uncertainty in temperature extraction as compared to widely-used CFM without sacrificing the 2 m spatial resolution of the sensors. Such reduced uncertainty can also be achieved by ultrafast processing of experimental BGSs acquired from BOTDA experiment. The effect of data interpolation on the performance of WMFD is also analyzed, which suggests that the speed in extracting temperature distributions by using WMFD can also be customized to attain special time requirements for particular applications. Thus, the proposed WMFD can be an effective alternative tool for highly accurate and ultrafast extraction of temperature distributions along the fiber which will make BOTDA sensors more suitable for real-world applications.

Acknowledgement

The experimental data processed in this study have been collected from the 'PolyU Photonics Research Center' at The Hong Kong Polytechnic University, Hong Kong SAR.

References

1. P. Lu, N. Lalam, M. Badar, B. Liu, B. T. Chorpening, M. P. Buric, and P. R. Ohodnicki, "Distributed optical fiber sensing: Review and perspective," *Appl. Phys. Rev.*, vol. 6, pp 1-35, 2019.
2. A. Motil, A. Bergman, and M. Tur, "State of the art of Brillouin fiber-optic distributed sensing," *Opt. & Laser Technol.*, vol. 78, no. A, pp 81-103, 2016.
3. D. Iida, N. Honda, and H. Oshida, "Advances in distributed vibration sensing for optical communication fiber state visualization," *Opt. Fiber Technol.* 102263, vol. 57, pp 1-9, 2020.
4. A. Coscetta, A. Minardo, and L. Zeni, "Distributed Dynamic Strain Sensing Based on Brillouin Scattering in Optical Fibers," *Sensors* 5629, vol. 20, no. 19, pp 1-23, 2020.
5. X. Angulo-Vinuesa, S. Martin-Lopez, P. Corredera, and M. Gonz'alez-Herr'aez, "Raman-assisted Brillouin optical time-domain analysis with sub-meter resolution over 100 km," *Opt. Express*, vol. 20, no. 11, pp 12147-12154, 2012.
6. S. Wang, Z. Yang, S. Zaslowski, and L. Th'evenaz, "Short spatial resolution retrieval from a long pulse Brillouin optical time-domain analysis trace," *Opt. Lett.*, vol. 45, no. 15, pp 4152-4155, 2020.
7. A. K. Azad, F. N. Khan, W. H. Alarashi, N. Guo, A. P. T. Lau and C. Lu, "Temperature extraction in Brillouin optical time-domain analysis sensors using principal component analysis based pattern recognition," *Opt. Express*, vol. 25, no. 14, pp 16534-16549, 2017.
8. A. K. Azad, L. Wang, N. Guo, H. Y. Tam and C. Lu, "Signal processing using artificial neural network for BOTDA sensor system," *Opt. Express*, vol. 24, no. 6, pp 6769-6782, 2016.
9. N. D. Nordin, M. S. D. Zan, and F. Abdullah, "Comparative Analysis of the Deployment of Machine Learning Algorithms in the Distributed Brillouin Optical Time Domain Analysis (BOTDA) Fiber Sensor," *Photonics* 79, vol. 7, no. 4, pp 1-13, 2020.
10. M. A. Soto, and L. Th'evenaz, "Modeling and evaluating the performance of Brillouin distributed optical fiber sensors," *Opt. Express*, vol. 21, no. 25, pp 31347-31366, 2013.
11. K. Yu, N. Guo, Z. Cao, S. Lou, C. Shang, and J. He, "Fast information acquisition using spectra subtraction for Brillouin distributed fiber sensors," *Opt. Express*, vol. 27, no. 7, pp 9696-9704, 2019.
12. A. K. Azad, "Analysis of 2D Discrete Wavelet Transform Based Signal Denoising Technique in Brillouin Optical Time Domain Analysis Sensors," *The Dhaka University JASE*, vol. 5, no. 1 & 2, pp 1-8, 2020.
13. M. A. Farahani, E. Castillo-Guerra, and B. G. Colpitts, "Accurate Estimation of Brillouin frequency shift in Brillouin optical time domain analysis sensors using cross correlation," *Opt. Lett.*, vol. 36, no. 21, pp 4275-4277, 2011.
14. X. Qian, X. Jia, Z. Wang, B. Zhang, N. Xue, W. Sun, Q. He and H. Wu, "Noise level estimation of BOTDA for optimal non-local means denoising," *Appl. Opt.*, vol. 56, no. 16, pp 4727-4734, 2017.
15. M. A. Soto, J. A. Ram'irez, and L. Th'evenaz, "Optimizing Image Denoising for Long-Range Brillouin Distributed Fiber Sensing," *J. Lightwave Technol.* vol. 36, no. 4, pp 1168-1177, 2018.
16. K. Luo, B. Wang, N. Guo, K. Yu, C. Yu, and C. Lu, "Enhanced SNR by Anisotropic Diffusion for Brillouin Distributed Optical Fiber Sensors," *J. Lightwave Technol.* vol. 38, no. 20, pp 5844-5852, 2020.
17. M. A. Farahani, E. Castillo-Guerra, and B. G. Colpitts, "A Detailed Evaluation of the Correlation-Based Method Used for Estimation of the Brillouin frequency shift in BOTDA sensors," *IEEE Sensors J.*, vol. 13, no. 12, pp 4589-4598, 2013.
18. M. A. Farahani, M. T. V. Wylie, E. Castillo-Guerra, and F. G. Colpitts, "Reduction in the number of averages required in BOTDA sensors using wavelet denoising techniques," *J. Lightwave Technol.* vol. 30, no. 8, pp 1134-1142, 2012.
19. M. A. Soto, J. A. Ram'irez, and L. Th'evenaz, "Intensifying the response of distributed optical fibre sensors using 2D and 3D image restoration," *Nat. Commun.* 10870, 7, pp 1-11, 2016.
20. M. A. A. El-Fattah, M. I. Dessouky, A. M. Abbas, S. M. Diab, E. M. El-Rabaie, W. Al-Nuaimy, S. A. Alshebeili, and F. E. A. El-Samie, 2014, "Speech enhancement with an adaptive Wiener filter," *Int. J. Speech Technol.*, 17, pp 53-64.
21. S. K. Jadwa, "Wiener Filter based Medical Image Denoising," *Int. J. Sci. & Engg. Applications*, vol. 7, no. 9, pp 318-323, 2018.
22. F. Wu, W. Yang, L. Xiao, and J. Zhu, "Adaptive Wiener Filter and Natural Noise to Eliminate Adversarial Perturbation," *Electronics* 1634, vol. 9, no. 10, pp 1-14, 2020.
23. C. R. Park, S. H. Kang, and Y. Lee, "Median modified Wiener filter for improving the image quality of gamma camera images," *Nuclear Engg. & Technol.*, vol. 52, no. 10, pp 2328-2333, 2020.
24. Z. Zhao, A. Zhao, J. Hui, B. Hou, R. Sotudeh, and F. Niu, "A Frequency-Domain Adaptive Matched Filter for Active Sonar Detection," *Sensors* 1565, vol. 17, no. 7, pp 1-12, 2017.
25. B. A. Odhavjibhai, and S. Rana, "Analysis of Matched filter based spectrum sensing in cognitive radio," *Int. Research J. Engg. & Technol.*, vol. 4, no. 4, pp 578-581, 2017.
26. S. Kalhor, F. A. Umrani, M. A. Khanzada, and L. A. Rahoo, "Matched Filter Based Spectrum Sensing for 4G Cellular Network," *Mehran Univ. Research J. Engg. & Technol.*, vol. 38, no. 4, pp 973-978, 2019.
27. J. P. Bailey, A. N. Beal, R. N. Dean, and M. C. Hamilton, "A digital matched filter for reverse time chaos," *Chaos* 073108, vol. 26, no. 7, pp 1-8, 2016.
28. A. K. Azad, "Effects of pump-pulse width and temperature on experimental Brillouin gain spectrum obtained from Brillouin optical time-domain analysis sensors," *Bangladesh J. Physics*, vol. 27, no. 1, pp 69-80, 2020.